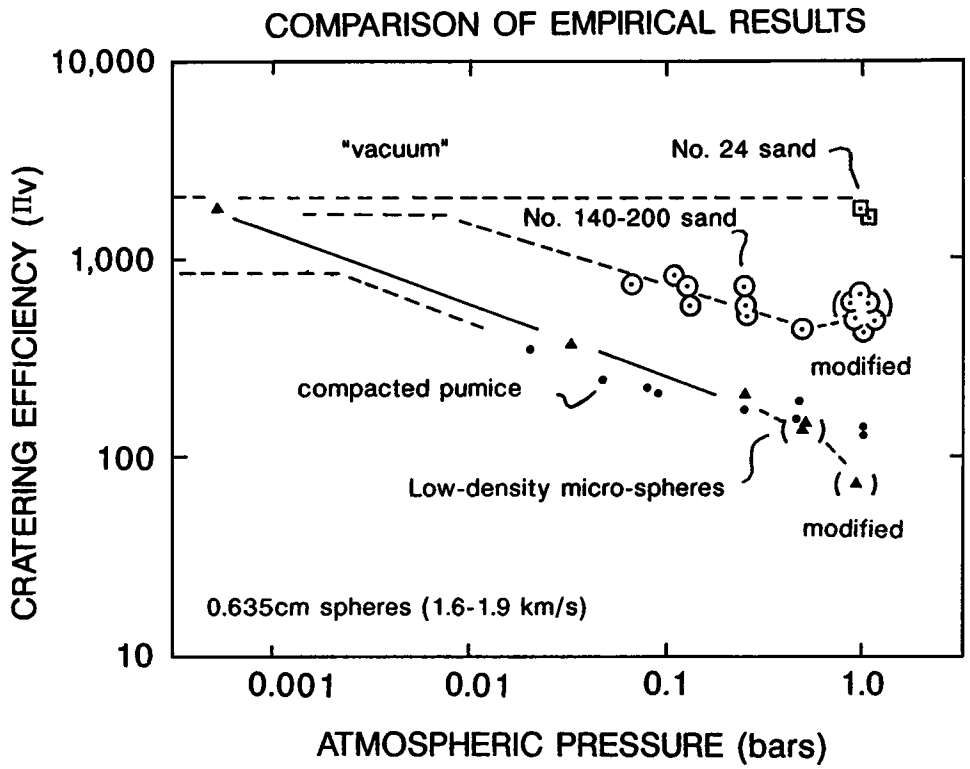

Fig. 3*a*. Comparison of empirical results for different target types with similar impactor conditions (0.635 cm diameter, 1.5-1.8 km/s). Cratering efficiency for pumice is generally less than for sand due to its greater interparticle cohesion. Nevertheless, atmospheric pressure has a similar effect on cratering efficiency regardless of extreme range in cohesion. Particle size apparently has a greater effect. Parentheses indicate that the final crater was modified by rim collapse and possibly other processes.

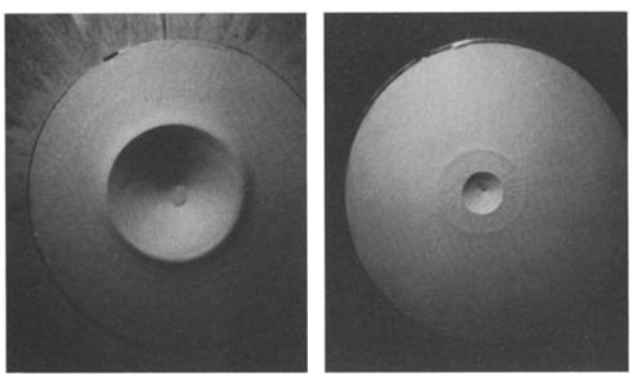

Fig. 3*b*. Comparison of craters formed under vacuum (left) and atmospheric (right) conditions for impacts into a target of low-density microspheres. In addition to a twenty fold decrease in cratering efficiency, the crater rim is observed to slump into the crater floor at late stages. Crater at left was formed by a 0.635-cm polyetheline sphere impacting at 1.5 km/s under 0.5 torr of a helium-purged chamber. The crater at right was formed by a similar impactor impacting at 1.20 km/s. The distinctive ejecta rampart is characteristic and is discussed in other contributions [*Schultz and Gault*, 1983; *Schultz*, 1987, 1991].

complications introduced by the projectile bow shock or wake (f_a in equation (1)). A subset of the total data set, therefore, is examined first: helium with $P < 1$ bar for low impact velocities but ≤ 0.25 bar at high velocities; other gases (air, carbon dioxide, argon) with $\rho/\rho_o \leq 0.5$ only at low impact velocities. In order to avoid transitional conditions at very low atmospheric pressures, all atmospheric pressures are high enough to cause about a factor of 2 reduction in cratering efficiency.

The first test concerns the possibility that compacted pumice should be characterized by strength-dominated scaling. Under vacuum conditions, the π_2 exponent α (equation (2)) closely resembles other particulate targets [*Schultz and Gault*, 1985] with both projectile size (factor of 20) and velocity (factor of 10) affecting cratering efficiency, in contrast with equation (9). Under atmospheric conditions, data expressed in terms of equation (9) can be plotted against atmospheric pressure for a given projectile size. The derived pressure exponent β can be used to correct the left side of equation (10*d*) in order to recognize any dependence on projectile size. Figure 4*a* reveals that cratering efficiency under helium at low impact velocities (2 km/s) decreases as pressures increase with $\beta = 0.23$. Experiments conducted in helium are shown in bold in order to emphasize this data set. Other gas compositions at low densities exhibit a very similar dependence with a possible departure at higher densities ($\rho/\rho_o > 0.25$). Here the strength-controlled exponent β' for pumice is assumed to be 0.63 on the basis of a value of the coupling exponent μ (≈ 0.42) derived from vacuum conditions. Figure 4*a* also shows that fine-grained no. 140-200 sand (with $\beta' = 0.58$ for $\mu \cong 0.39$) exhibits essentially the same pressure dependence, even though the static cohesion properties are dramatically different for the two materials. Figure 4*b* shows that the pressure-corrected, strength-scaled cratering efficiency depends on projectile size, contrary to equation (9).